A BUOYANT TURBULENT AIR JET DISCHARGED AT ARBITRARY ANGLE TO THE SURROUNDINGS

A.A. Abdel-Rahman*

Mechanical and Industrial Engineering Department, College of Engineering,
Kawait University, Kuwait.

ABSTRACT

An experimental investigation has been undertaken to study the mean and turbulent fields of a buoyant plane turbulent air jet discharged at various angles to quiescent surroundings. The buoyancy was generated by discharging heated air through a 60 cm x 1 cm nozzle. A buoyancy induced streamline curvature was produced by tilting the jet away from the vertical. The jet flow was studied for jet discharge angles of 0, 22.5 and 45°, each for two exit Froude numbers; $Fr_o = 796$ and 1453. Profile measurements of the mean flow and turbulence quantities were made at downstream stations up to 75 nozzle widths. Measurements were performed using hot-wire anemometry. A unique feature of the present data is that traverses were made normal to the mean curved path of the jet. The results reveal that the mean flow field is largely unaffected by buoyancy forces or discharge angle, while the turbulence shear stress and transverse heat flux are most affected.

1. INTRODUCTION AND BACKGROUND

Many turbulent flows of practical significance are subject to the interaction of buoyancy and curvature which influence the turbulence structure, and consequently, the gross characteristics of the flow. Prediction of such flows is presently limited by the accuracy of available turbulence models (c.f. Rodi, 1982; Gibson, 1978; Gibson and Launder, 1976), and the lack of experimental data (c.f. Chen and Rodi, 1980). The present study is an attempt to enhance the understanding of turbulent free flows with buoyancy induced curvature, and ultimately, to provide experimental data to aid in the development of prediction methods.

The basic flow of curved buoyant discharge has been studied by Chan and Kennedy (1975), Anwar (1969) and Abraham (1965), however, their studies focussed only on the jet trajectory. Oosthuizen and Lemieux (1984) undertook an experimental study on the structure of a heated slot jet flow. They investigated the influence of the jet discharge angle on the jet flow for exit Froude numbers of 769 and 1429. Tests were conducted for discharge angles of 0, 30, 60 and 90°. They concluded that the mean velocity and temperature profiles are nearly self-similar except for some asymmetry in the inclined jets. They found that buoyancy has a significant effect on the transverse normal turbulence stress, shear stress and transverse heat flux where their values reduced on the thermally stable side (convex side, see Figure 1) of the jet. There are some points, however, to be noted: (i) their traverses were made normal to the jet discharge direction, rather than the jet trajectory. As a result, only the x-component of the streamwise velocity was measured. In addition, this traverse method has likely caused misalignment between the probe axis and the jet center-line thus, introducing a source of error associated with the yaw sensitivity of the X-wire. It was shown (Verriopoulos, 1983) that such misalignment will result in an error of the measured quantities; being greatest in the measured shear stress. (ii) They used the "cosine" cooling law in their X-wire analysis; which has been shown to be less reliable for flows of low velocity or high turbulence levels (c.f. Bruun and Tropea, 1985; Hinze, 1975; Bruun, 1972; Bradshaw, 1971 and Champagne et al, 1967).

The main objective of the present work is to provide a detailed data base that will confirm and enhance the Oosthuizen and Lemieux experiments, and provide a basis for better understanding the effects of buoyancy and curvature. Two essential measurement

* On leave from the Faculty of Engineering, Alexandria University, Alexandria, Egypt.

considerations were undertaken to improve the accuracy of the hot-wire results. First, a comprehensive technique incorporated both yaw and temperature sensitivities was used (Abdel Rahman et al 1989).

Second a procedure adopted (described later) to traverse the hot-wire probes in accordance with the s, n plane of the jet flow (see Figure 1), thus, minimizing the misalignment, and the associated error, between the probe axis and jet center-line.

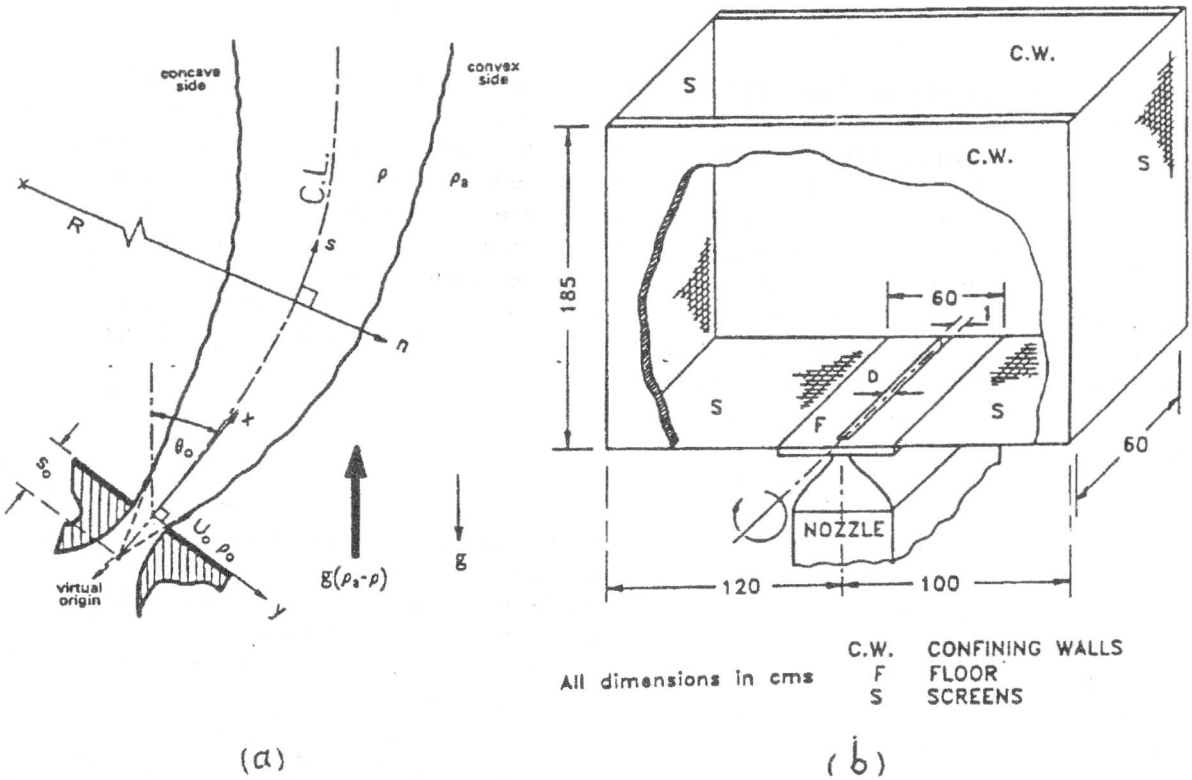

Figure 1: (a) A curved buoyant plane Jet: definition sketch and coordinate axes
(b) Layout and dimensions of the jet enclosure.

2. EXPERIMENTAL APPARATUS

The apparatus consists of a variable speed centrifugal blower which provides the airflow through a 3.7m long round flexible duct and a 1m diffuser section, to a 40cm x 60cm x 12.5cm settling chamber, followed by a corner section containing 90° turning vanes, a second shorter settling chamber and finally a 40:1 contraction which ends as a 60cm x 1cm slot. The nozzle exit turbulence intensity was less than $\approx 0.7\%$. Profile measurements of the mean velocity and turbulence intensity at the nozzle exit indicate that the wall boundary layers at the exit are laminar (e.g. Hussai and Clark, 1977). The vertically exiting jet is enclose by a horizontal floor extending along the length of th slot and 30 cm on each side as shown in Figure (1) The jet is confined by two vertical walls placed at eac end of the slot. The entrained air passed through 0. aspect ratio screens spanning the ends of the confini walls. Th mean flow was two-dimensional expect in th vicinity of the walls. The jet flow can be uniformly heated to a maximum of $\approx$ 100°C at a nominal ex

velocity of 4 m/s. The electric heater has an output capacity of 6.25 kW and consists of a network of 16.5 cm of 14 gauge Hoskins Crome-A wire mounted in a ceramic tube upstream of the diffuser section. The exit temperature can be maintained constant with a temperature controller to within ± 1 °C. Additional features of the apparatus include, filtering of the air at both the inlet and the outlet of the blower, vibration isolation of the motor-blower assembly, insulation of the apparatus to minimize heat loss to the surroundings, winch and wire rope arrangement to enable tilting the apparatus for inclined jet experiments, and automatic probe traversing.

2.1 Experimental conditions

The jet was studied for three jet discharge angles, namely 0, 22.5 and 45° to the vertical. For each discharge angle two experiments were conducted each at a different exit Froude number, Fr_o = 796 and 1453, which correspond to an exit temperature $T_o \approx$ 100°C and exit velocities U_o = 4.5 and 6.2 m/s respectively. The exit to ambient density ratio ρ_o/ρ_a, was kept fairly constant for all the experiments and Reynolds number ranged between 1880 and 2600. The actual experimental conditions are given in Table (1).

Table 1. Exit conditions of experiments.

run no.	U_o, m/s	ΔT_o, °C	θ_o, deg.	Fr_o	T_a, °C	$\frac{\rho_o}{\rho_a}$
A1	6.16	78.5	00.0	1456	22.0	.79
A2	4.49	76.5	00.0	805	22.5	.80
B1	6.20	79.0	22.5	1451	22.0	.79
B2	4.50	77.0	22.5	792	23.0	.79
C1	6.20	79.5	45.0	1453	21.0	.79
C2	4.49	76.5	45.0	790	21.5	.79

3. MEASUREMENT TECHNIQUES, INSTRUMENTATION AND SIGNAL ANALYSIS

The measurement of the jet was facilitated by a computer controlled traversing mechanism. The traversing mechanism, mounted on the side of the slot major axis, can be tilted in the x,y plane up to 45° to the horizontal with a resolution of 0.5° to permit traversing in the s,n plane. The probes can be moved in the s, n and z directions to within 0.01 mm 0.01 mm and 0.5 mm respectively. Since the traverses in the tilted jet cases were to be made in the s, n plane; i.e., along lines normal to the jet trajectory, the jet trajectory first had to be found. This trajectory, to be discussed later, was then used to calculate the required traversing lines for all downstream measurement stations.

The measurements were taken with a triple-wire probe arrangement comprising an X-array wire probe and a cold wire probe. The sensor of the cold wire was located slightly upstream form the X-wire sensors to avoid their thermal wake. The X-Wire is a standard DISA 55P51 gold-plated tungsten, connected to a DISA 56C01 system through two 56C16 general purpose bridges for velocity measurements. The cold wire is a 1μm platinum wire, operated in the constant current mode and connected to a 56C20 temperature bridge. The analog signals from the X-array wires were passed through a signal conditioner and then simultaneously sampled, together with the analog signal from the cold wire using a multichannel, high speed 12 bit A/D converter interfaced under DMA control to a IBM PC-XT. The raw data were stored on magnetic tape and then read back and analyzed.

The hot-wire signals were interpreted using the heat transfer response equation given by Collis and Williams, 1959

$$Nu \left(\frac{T_m}{T_a}\right)^{-.17} = A + B\,Re^{n} \qquad (1)$$

for .02 < Re < 44. Nu and Re are the Nusselt number and Reynolds number of the wire and can be expressed as

$$Nu = \frac{E^2}{\pi \iota R_s k_s (T_s - T_a)} \qquad (2)$$

and

$$Re = \frac{\rho U d}{\mu} \qquad (3)$$

and ρ,μ, and k_s, are the density , viscosity and thermal conductivity of the air film around the wire respectively, whereas, R_s and E are the sensor operating resistance and output voltage respectively. Equation (1) was chosen, mainly because it represents a physical heat transfer model for the hot-wire, rather

than just a regression model, which was shown to form the basis for complete separation of temperature and velocity effects on the hot-wire signals with no further temperature calibration (Abdel-Rahman et al, 1987). Also, the statistical uncertainties in the coefficients A, B and n are quite reasonable (Swaminathan et al, 1986), particularly, for velocities below 20 m/s (Bruun, 1971). Accounting for the yaw sensitivity of the X-wire is essential, especially, for flows of high turbulence levels or low velocities. Bruun and Tropea (1985), presenting a summary of the available approaches which account for such a sensitivity, suggested that a digital technique incorporating the yaw dependence of A,B and n should be used, particularly for flows with high turbulence intensities. Such an approach of making A, B and n functions of the yaw angle, α, has been adopted in the present study. A complete velocity calibration was, therefore, carried out at all desired yaw angles over the range 0° to 90°. A regression analysis was then applied for each value of α, using equation (1), to determine the yaw dependence of A, B and n. Having determined these coefficients for each value of α, equation (1) could be written as:

$$Nu \left(\frac{T_m}{T_a}\right)^{-.17} = A(\alpha) + B(\alpha) Re^{n(\alpha)} \qquad (4)$$

Equation (4), now accounting for the yaw and temperature sensitivities, and the cold wire response equation

$$E_t = C_{t1} + C_{t2}\, T \qquad (5)$$

were implemented in an iterative digital signal analysis technique to solve for the instantaneous velocity vector and instantaneous temperature (T), rather than statistical quantities ($\bar{U}, \bar{V}, \bar{T}, \overline{u^2}, \overline{ut}$, etc). The idea of the technique is to guess the flow direction, ϕ, and calculate the velocity values from both sensors of the X-wire, and repeat this process after changing ϕ by small increment, $\Delta\phi$, till both velocities converge to within 2%. At this point the magnitude of the instantaneous velocity, U_{tot}, is taken to be the arithmetic average of both, and the flow direction is given by the angle, ϕ, at which convergence is achieved. The final result from the analysis technique is an instantaneous velocity vector (U_{tot}, ϕ) and accompanying instantaneous temperature, T. Knowing the instantaneous values of temperature and velocity, it is straight forward to calculate any statistical quantity using standard statistical operations. An accuracy test of the technique in resolving the flow direction and velocity gave quite acceptable results. Details of the accuracy test as well as calibration and analysis of X-wire signals can be found in Abdel-Rahman et al (1989). An implicit assumption in the analysis technique was that both sensors of the X-wire sense the same velocity vector.

3.1 Experimental uncertainties

Details of careful precautions taken to keep uncertainty of measurements to a minimum as well as uncertainty analysis are given in Abdel-Rahman (1987). The estimated uncertainty associated with the measured quantities are included in Table (2).

4. RESULTS AND DISCUSSION

To calculate the n-direction traverse lines for the tilted jet cases, lateral traverses in the y-direction were made, using Pilot tube and cold wire probes, to measure the mean velocity and temperature profiles. The displacement of the positions of maximum velocity was found, and the locus of these positions gave the jet trajectory[1]. The measured trajectories of the jet flow for all discharge angles and exit Froude numbers are given in Figure (2). To allow direct comparison, these trajectories are replotted in Figure (3) after normalization with respect to an axis coincident with the discharge angles. As seen in this Figure, the upward displacement of the trajectory increases with the increase of discharge angle and decrease of exit Froude number. The trajectories used by the computer to calculate the traverses in the s,n plane, shown by solid lines, are empirical fit to the data according to

$$y = a_1 x + a_2 x^{1.5} + a_3 x^2 + a_4 x^{2.5} \qquad (6)$$

The curvature of the jet trajectory, R, was calculated using the equation

1. The jet trajectory based on the temperature field was found to be similar but slightly above that based on the velocity field. The jet trajectory was considered to be represented by that given by the velocity field.

Table 2. Uncertainties associated with the measured quantities

quantity	uncertainty
$\bar{U}$	±2%
$\bar{V}$	±3%
$\Delta\bar{T}$	±1.5%
$\sqrt{\overline{u^2}}$	±4%
$\sqrt{\overline{v^2}}$	±6.5%
$\sqrt{\overline{t^2}}$	±4%
$\overline{uv}$	±9%
$\overline{ut}$	±8%
$\overline{vt}$	±10%

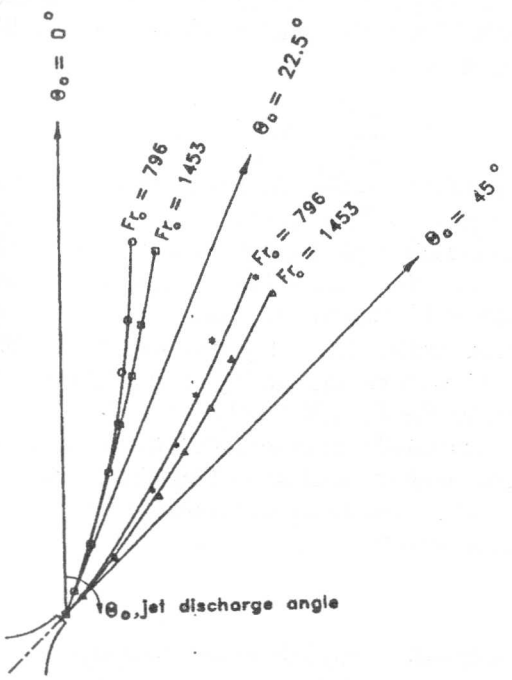

Figure 2. Measured trajectories of the jet flow.

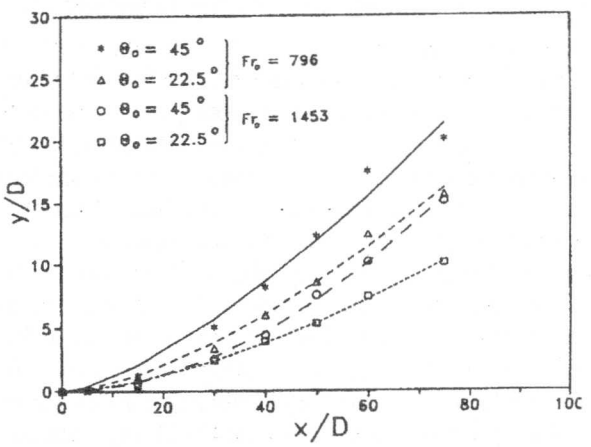

Figure 3. Comparison of jet trajectories for different discharge angles and exit Froude numbers.

$$R = \frac{(1 + (dy/dx)^2)^{3/2}}{d^2y/dx^2} \qquad (7)$$

together with equation (6). The sense of curvature of the jet flow is demonstrated in Figure (4) where b/R is plotted against s/D and b is the velocity half-width, to be described later in the paper.

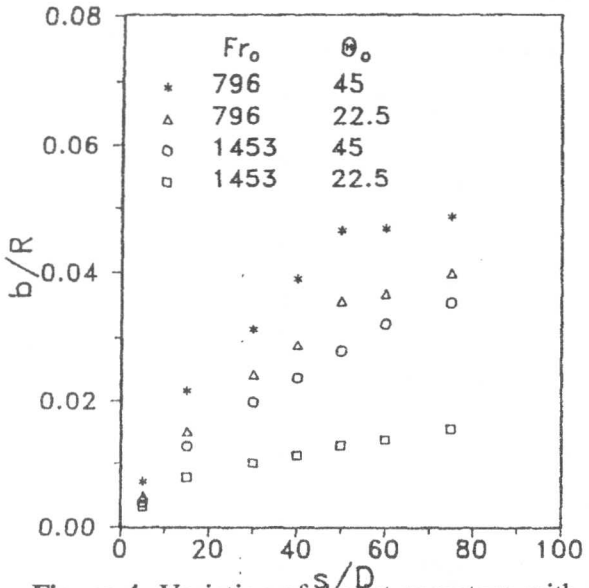

Figure 4. Variation of the jet curvature with downstream direction.

4.1 Mean flow

Profile measurements of

$\bar{U}, \bar{V}, \Delta\bar{T}, \overline{u^2}, \overline{t^2}, \overline{uv}\ \overline{ut}$ and $\overline{vt}$ were made at downstream stations (s/D's) up to 75 nozzle widths.

Typical profiles of the longitudinal mean velocity, $\bar{U}$, and mean temperature, $\Delta\bar{T}$, for a nominal exit Froude number of 1453 are shown in Figure (5). The data are normalized by the scales at the exit plane. It is clearly seen that for a given Froude number, the mean velocity and temperature fields are insensitive to the discharge angle θ_o and geometrically similar. Figure (6) demonstrates that for a given discharge angle, θ_o, the buoyancy force has a very slight effect on both the velocity and temperature fields. It can be observed from Figure 6 (a) that there is a slight increase in the mean velocity with increasing buoyancy force (decreasing Froude number). This increase in the mean velocity becomes more noticeable with the increase of s/D where buoyancy force becomes comparable with the inertia force. In Figure 6 (b), a very slight decrease in the mean temperatures is seen, particularly for the far s/D stations, but within the experimental uncertainty.

All profiles of all runs display symmetry around the jet center-line. Such a symmetry is best illustrated by Figure (7) where the negative sides of the velocity and temperature profiles are folded over upon the positive side. It can be concluded, then that mean velocity and temperature profiles are symmetric around the jet center-line and largely unaffected by either buoyancy or discharge angle (curvature).

Demonstration of self-similarity of the mean velocity and temperature profiles is shown in Figure (8) where the data are normalized by the similarity scales: $\bar{U}_c, \Delta\bar{T}_c$, b and b_t. All profiles, for s/D $\geq$ 15, exhibit a good degree of self-similarity, and fall well on the universal Gaussian profile expect near the edges where slightly higher values of velocities and temperatures are observed. These high values are due to the larger experimental uncertainties there, where velocities and temperatures are small as well as turbulence level is high.

Center-line decay of longitudinal mean velocity is shown in Figure (9). The decay constants A's, included in Table (3), were calculated by fitting the data to

$$\frac{\bar{U}_c}{U_o} = A\left(\frac{s}{D} - \frac{s_{od}}{D}\right)^{-1/2} \qquad (8)$$

For the temperature field, the center-line decay is shown in Figure (10) and the decay constants, B's, are calculated from

$$\frac{\Delta\bar{T}_c}{\Delta T_o} = B\left(\frac{s}{D} - \frac{s_{od}}{D}\right)^{-1/2} \qquad (9)$$

and reported in Table (4). The dynamic virtual origin, S_{od} in equations (8) and (9) is not necessarily the same. It is noticeable from Figure (9) and Table (3) that the decay of the center-line velocity, within the experimental uncertainty, are unaffected by the discharge angle. The buoyancy forces, on the other hand, show an effect; the higher the buoyancy forces (the lower the Froude number) the slower the decay (the higher the decay constant). This observation does not agree with the finding of Oosthuizen and Lemieux (1984), where the decay was found to increase with the buoyancy forces.

2. To accurately calculate the center-line values of longitudinal mean velocity and velocity half-widths, the data points for every transverse profile whose values are 0.4 of the maximum or larger was fitted to a 5th degree polynomial. Same method was used with the temperature profiles.

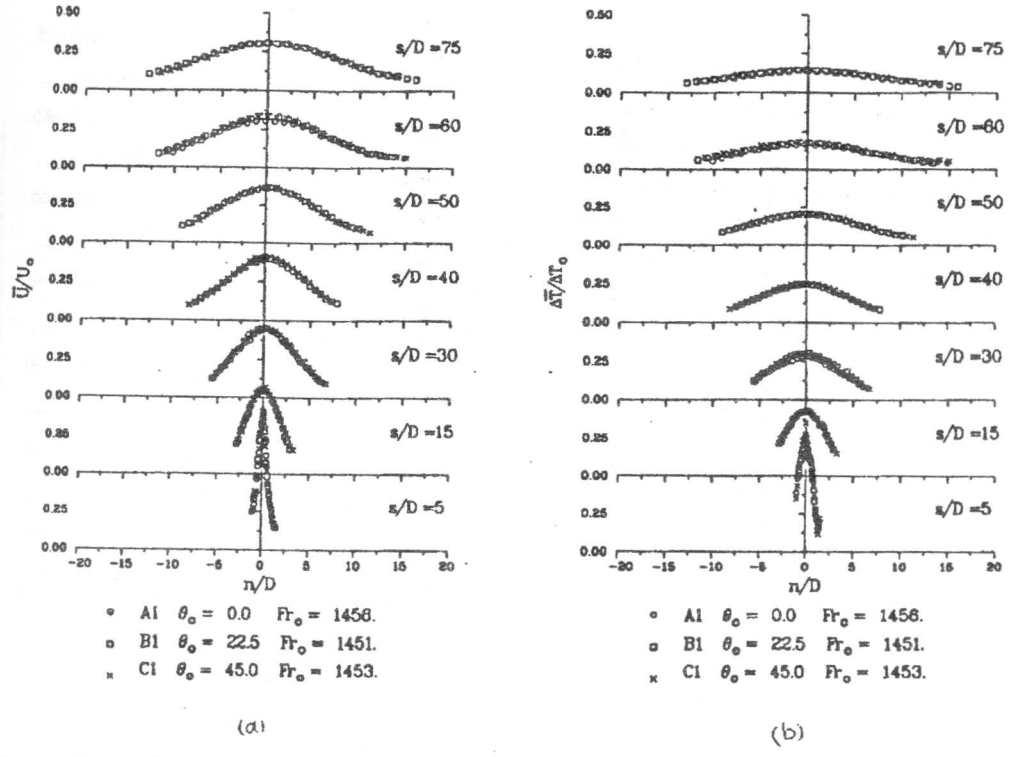

Figure 5: (a) Longitudinal mean velocity profiles, normalized by the jet exit velocity. (b) Mean temperature profiles, normalized by the jet exit temperature.

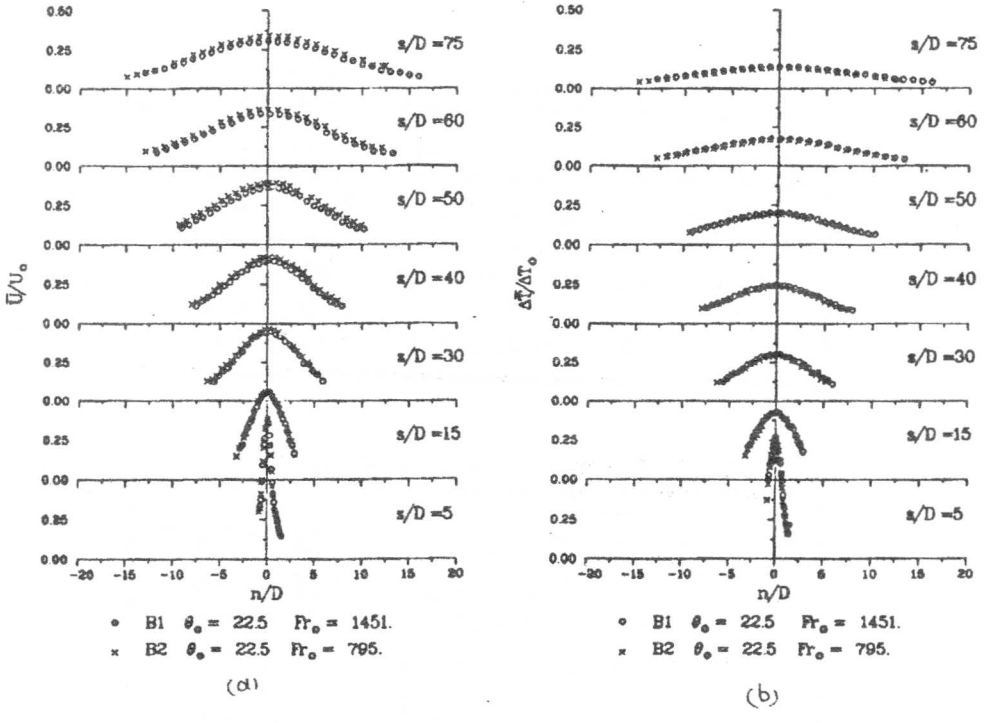

Figure 6: (a) Longitudinal mean velocity profiles, normalized by the jet exit velocity. (b) Mean temperature profiles, normalized by the jet exit temperature.

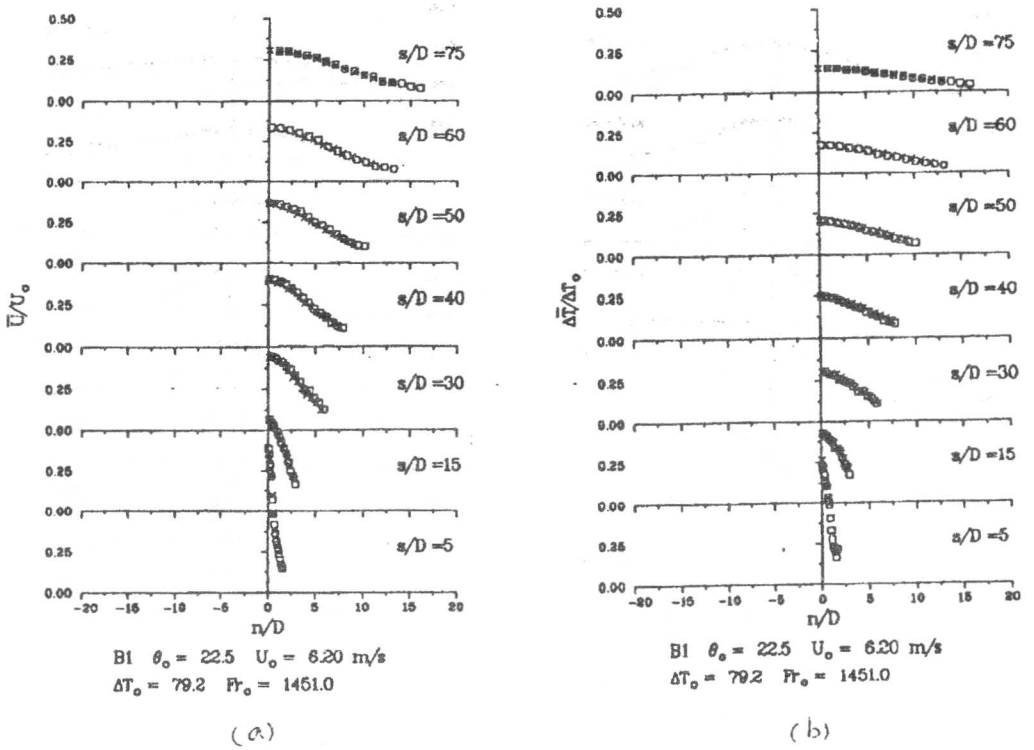

Figure 7: Longitudinal mean velocity and temperature profiles, illustrating the symmetry around the jet center line.
(a) Mean velocity profiles (b) Mean temperature profiles.

Table 3. Velocity decay constants.

run	A
A1 (Fr_o = 1453, θ_o = 00.0°)	2.35 ± 0.12
B1 (Fr_o = 1453, θ_o = 22.5°)	2.38 ± 0.12
C1 (Fr_o = 1453, θ_o = 450.0°)	2.35 ± 0.12
A2 (Fr_o = 796, θ_o = 00.0°)	2.65 ± 0.12
B2 (Fr_o = 796, θ_o = 22.5°)	2.70 ± 0.12
C2 (Fr_o = 796, θ_o = 45.0°)	2.57 ± 0.12

Table 4. Temperature decay constants.

run	B
A1 (Fr_o = 1453, θ_o = 00.0°)	1.39 ± 0.09
B1 (Fr_o = 1453, θ_o = 22.5°)	1.38 ± 0.09
C1 (Fr_o = 1453, θ_o = 45.0°)	1.44 ± 0.09
A2 (Fr_o = 796, θ_o = 00.0°)	1.24 ± 0.09
B2 (Fr_o = 796, θ_o = 22.5°)	1.23 ± 0.09
C2 (Fr_o = 796, θ_o = 45.0°)	1.15 ± 0.09

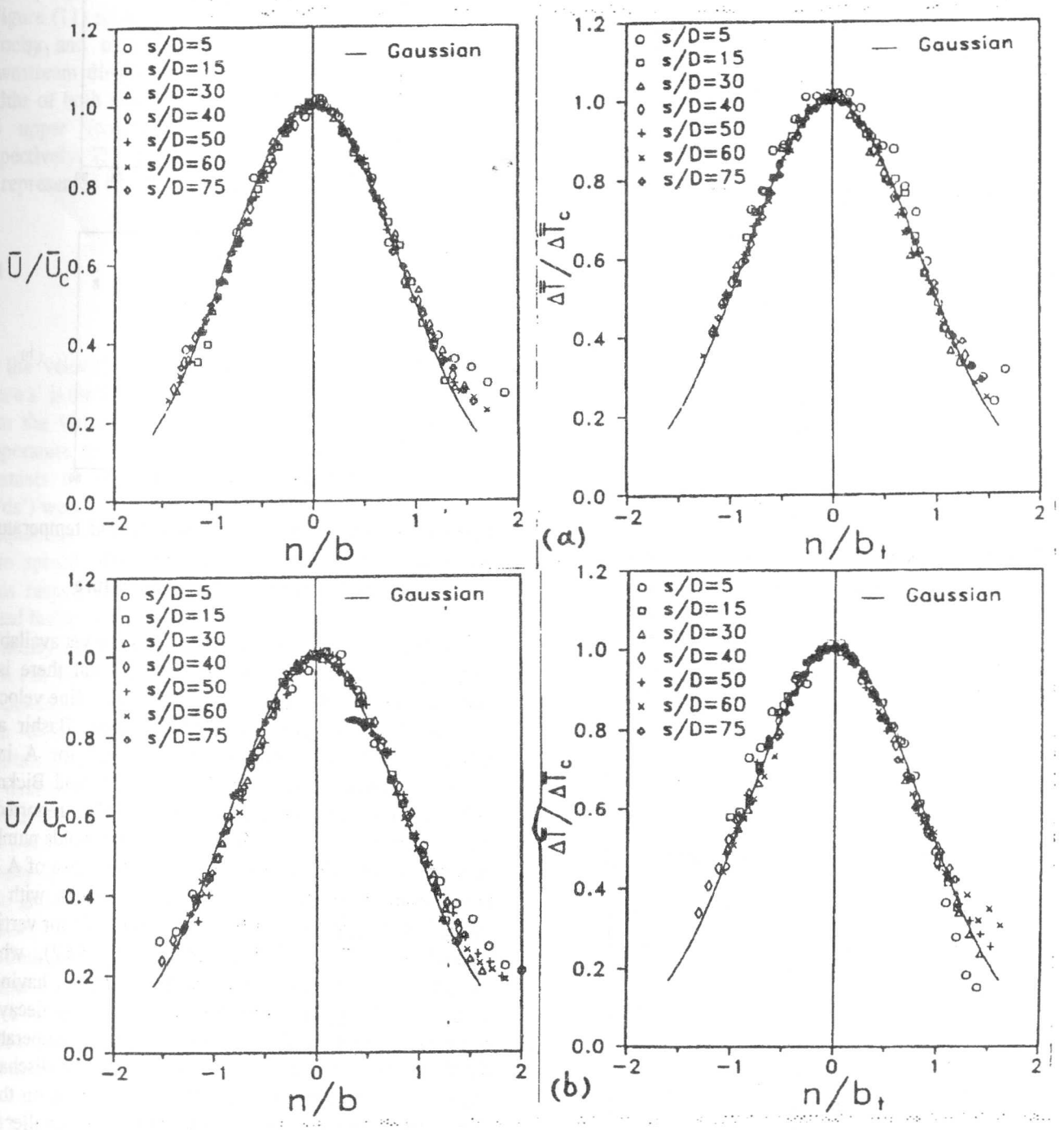

Figure 8: Self-similarity of longitudinal mean velocity and temperature profiles.
(a) run B1 (b) Run C1.

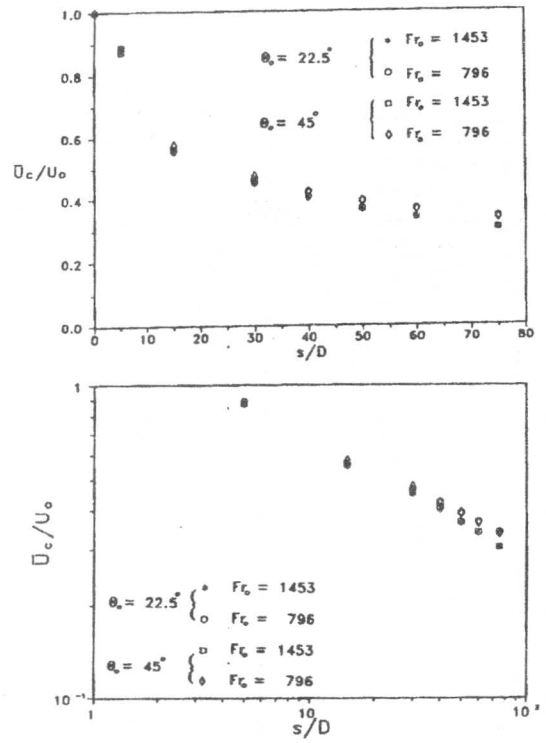

Figure 9. Decay of center-line mean velocity.

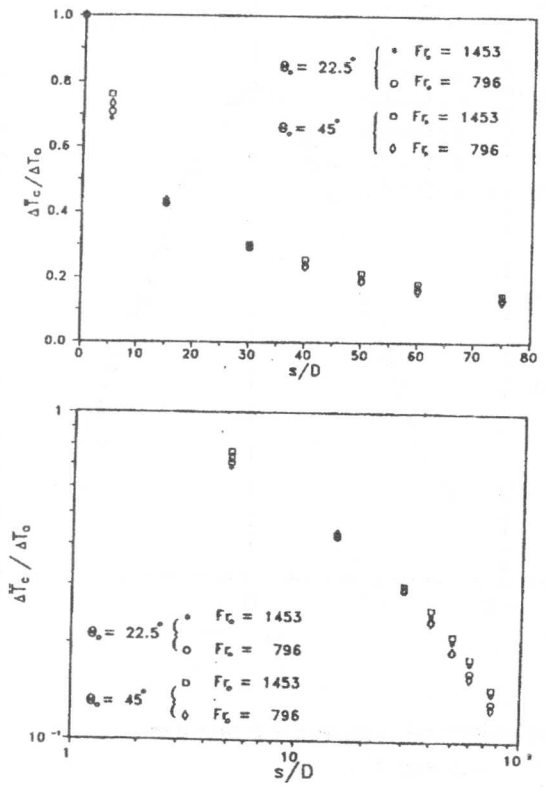

Figure 10. Decay of center-line mean temperature difference.

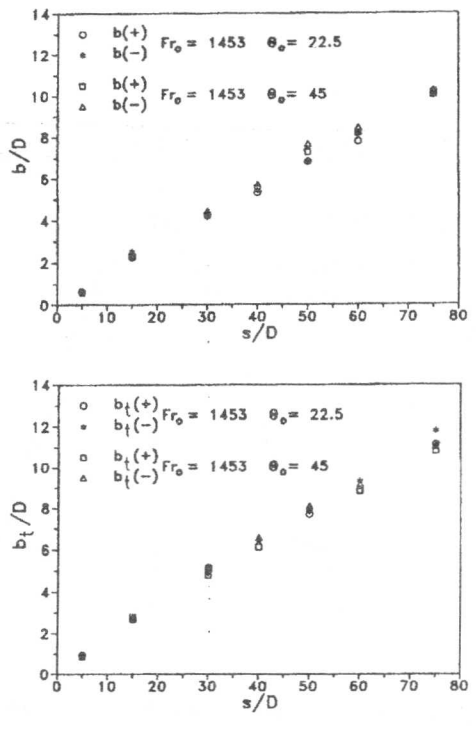

Figure 11. Development of velocity and temperatur half-widths in the downstream direction.
(a) Velocity (b) Temperature

A satisfactory explanation for this is not yet available The published data, however, reveal that there is considerable scatter in the decay of center-line velocit for jet flows in general. For example, Bashir an Uberoi (1975) obtained a value of 2.7 for A in slightly heated vertical jet (Fr_o=37284) and Bicknel (1937), refer to Chen and Rodi (1980), reported much higher value of 3.98 for a high Reynolds numbe isothermal jet. Table (3) shows that the value of A fo the vertical run (A1) is in good agreement with th value 2.4, recommended by Chen and Rodi for vertica heated jets. That of the vertical run (A2), whe buoyancy forces are larger, does not agree, having value of 2.65 ± .12. Similar to the velocity decay, i is observed that the decay constants of the temperatur field are almost the same for the different discharg angles. The buoyancy force shows an effect on thes constants; the stronger the buoyancy the smaller th constants (faster decay). The decay constants for th vertical runs, are found to be lower than those in th literature. Reardon found a value of 1.56 for his Fr_o = 2700 jet. Lemieux obtained an average value of 1.4 fo his Fr_o = 769 experiments and a value of 1.77 for th

Fr_o = 1429 experiments, while we obtain values of 1.39 and 1.24 for the cases of Fr_o = 1453 and 796 respectively.

Figure (11) shows typical developments of the local velocity and temperature half-widths (b,b_t) in the downstream direction, s. The figure shows the half-widths of both sides of the flow; b (-) and b (+) for the upper (concave) and lower (convex) sides respectively. The development is fairly linear and can be represented by

$$\frac{b}{D} \alpha \frac{s'}{D} \qquad (10)$$

and

$$\frac{b_t}{D} \alpha \frac{s'}{D} \qquad (11)$$

for the velocity and temperature fields respectively. where s′ is the distance along the center-line, measured from the virtual origin of the jet. The velocity and temperature spread rates, given by the proportionality constants of equations (10) and (11) (db/ds′ and db_t/ds') were calculated by fitting the local half-widths to equations (10) and (11). Table (5) and (6). contain these spread rates for the velocity and temperature fields respectively. The temperature field is seen to spread faster than the velocity field, and the half-widths are nearly equal on either side of the jet. From Table (5) it can be observed that the velocity spread rate is independent of buoyancy and discharge angle; all cases seem to have the same spread rate within the uncertainty of calculating db/ds′ (±5%). The spread of the temperature field, on the other hand, shows a dependence on the discharge angle, see Table (6) where the spread rate shows an increase with θ_o. The velocity spread rates of the vertical runs, A1, and A2, are slightly higher than the value recommended for the vertical buoyant jets. (.11) (Chen and Rodi 1980). Reardon (1985), for vertical buoyant jet of Froude number of 2700, found this value to be .123. Bashir and Uberoi (1975) obtained a value of .138 for a vertical jet with Froude number of 37284 and density ratio of .83. Lemieux (1983) for tilted buoyant jets got an average value, for all the discharge angles covered, of .128. He found that this value is applicable to both buoyant jets of Fr_o = 1429 and 769. For the temperature field, the spread rates of the vertical runs compare well with .14, as recommended by Chen and Rodi (1980). It is to be pointed out that the temperature spread rate shows a relatively wide band of scatter in the previous reported studies on vertical buoyant jets. That was attributed, by some authors, to the relative difficulty in measuring the temperature field. While Davis et al (1975) obtained a value of .125, Bashir and Uberoi (1975) got a value of .164 and Reardon (1985) found this value to be 0.154. Lemieux (1983) obtained a values of .19; he attributed such a high value to the low Reynolds number effects. Rajagopalan and Antonia (1980), realizing the difference in the jet spread rate among researches suggested that this difference may be related to one or a combination of the following: (a) the initial conditions, laminar or turbulent, (b) the flow field around the jet flow; e.g., drafts in the surrounding air, presence of solid boundaries like confining walls, floor or screens may influence the spread rate, and (c) the turbulence level at the jet exit. In summary, the velocity spread rate is found to be independent of buoyancy and discharge angle, whereas the temperature spread rate is somewhat dependent on the discharge angle only. The values of the velocity spread rates, found in the present study, are believed to have been affected by the low exit Reynolds number. Otugen and Namer (1986) showed that the jet spreads more rapidly with decreasing exit Reynolds number.

Table 5. Velocity spread rate.

run	db/ds′ (+)	db/ds′ (-)
A1 (Fr_o = 1453, θ_o = 00.0°)	.135	.132
B1 (Fr_o = 1453, θ_o = 22.5°)	.131	.131
C1 (Fr_o = 1453, θ_o = 45.0°)	.127	.124
A2 (Fr_o = 796, θ_o = 00.0°)	.131	.133
B2 (Fr_o = 796, θ_o = 22.5°)	.129	.129
C2 (Fr_o = 796, θ_o = 45.0°)	.140	.140

Table 6. Temperature spread rate.

run	db_t/ds' (+)	db_t/ds' (-)
A1 (Fr_o = 1453, θ_o = 00.0°)	.135	.136
B1 (Fr_o = 1453, θ_o = 22.5°)	.134	.141
C1 (Fr_o = 1453, θ_o = 45.0°)	.161	.162
A2 (Fr_o = 796, θ_o = 00.0°)	.138	.139
B2 (Fr_o = 796, θ_o = 22.5°)	.133	.132
C2 (Fr_o = 796, θ_o = 45.0°)	.161	.156

Typical transverse mean velocity profiles are shown in Figure (12).

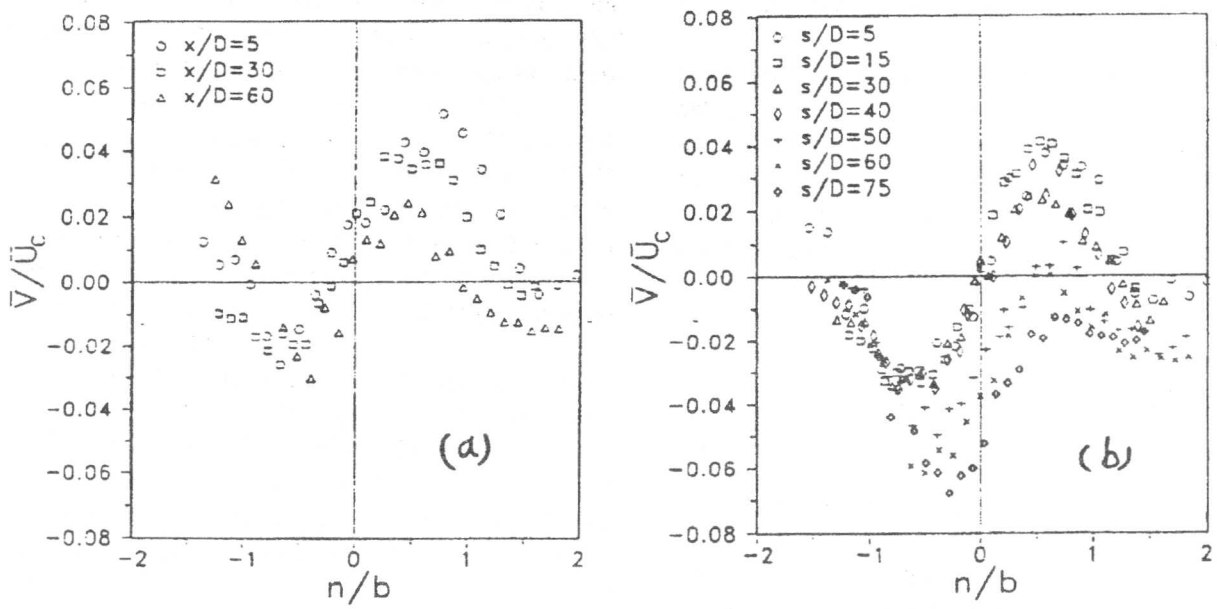

Figure 12. Transverse mean velocity profiles, normalized by the center-line mean velocity. (a) run A1 (b) run C1.

The values of $\bar{V}$ may not be very accurate since they are very small (in the order of few cm/s). The profiles of the vertical run (A1) do not exhibit self-similarity, however, they display the same shape and change sign from one side of the jet to the other. The maximum values of the profiles and the location where they cross the horizontal axis are comparable with those of the isothermal plane jets (e.g. Gutmark and Wygnaski; 1976). The outer regions of the profiles for the vertical case indicate that the entrainment rate increases in the streamwise direction. For case C1 ($\theta_o = 45°$) profiles for s/D > 40 show that the value of $\bar{V}$ on the thermally stable side (+ ve side of the horizontal axis) start decreasing and change sign, while on the unstable side, they start increasing. At this point it should be pointed out that Schwartzbach (1972), in his experiments on a reattaching jet flow, reported that for extreme stabilities the dependence of entrainment on curvature becomes inconsistent, and might even change sign.

4.2 Turbulence structure

Profiles of longitudinal turbulence intensity as well as its variation along the jet center-line are shown in Figure (13). It is seen that the profiles are fairly symmetrical w.r.t. jet center-line, and turbulence level is very much the same, thus showing no dependence on the discharge angle/buoyancy. The profiles peak off center-line, however, not as high as in isothermal jets. It is clear that the center-line turbulence intensity (bottom graph) levels off at $\approx$ 20% for s/D $\geq$ 30. Such a value of turbulence intensity agrees with that for high Reynolds number isothermal jets. The expected increase in the value due to buoyancy seems to have been masked by the low Reynolds number effects (Lemieux and Oosthuizen 1984, Otugen and Namer 1986). At s/D = 5, the turbulence level shows high values (44 → 50%). Such high values of turbulence intensity may be due, in part, to the buoyancy forces effects and, in part, to the interaction of the two shear layers on each side of the potential core. Another reason may be that the vortex shedding from the X-wire prongs has frequencies in the range of the dominating frequencies of the fluctuating field, thus resulting in an increase in the turbulence intensities (see Buresti and Cocco, 1987).

The transverse turbulence intensity profiles and its center-line variation are shown in Figure (14). Again, as was seen for the longitudinal intensity, the profiles in the far field have similar and symmetric shape around the center-line, indicating independence of buoyancy/discharge angle. It can be seen that the center-line variation does not level off; showing a slight gradual increase in the downstream direction.

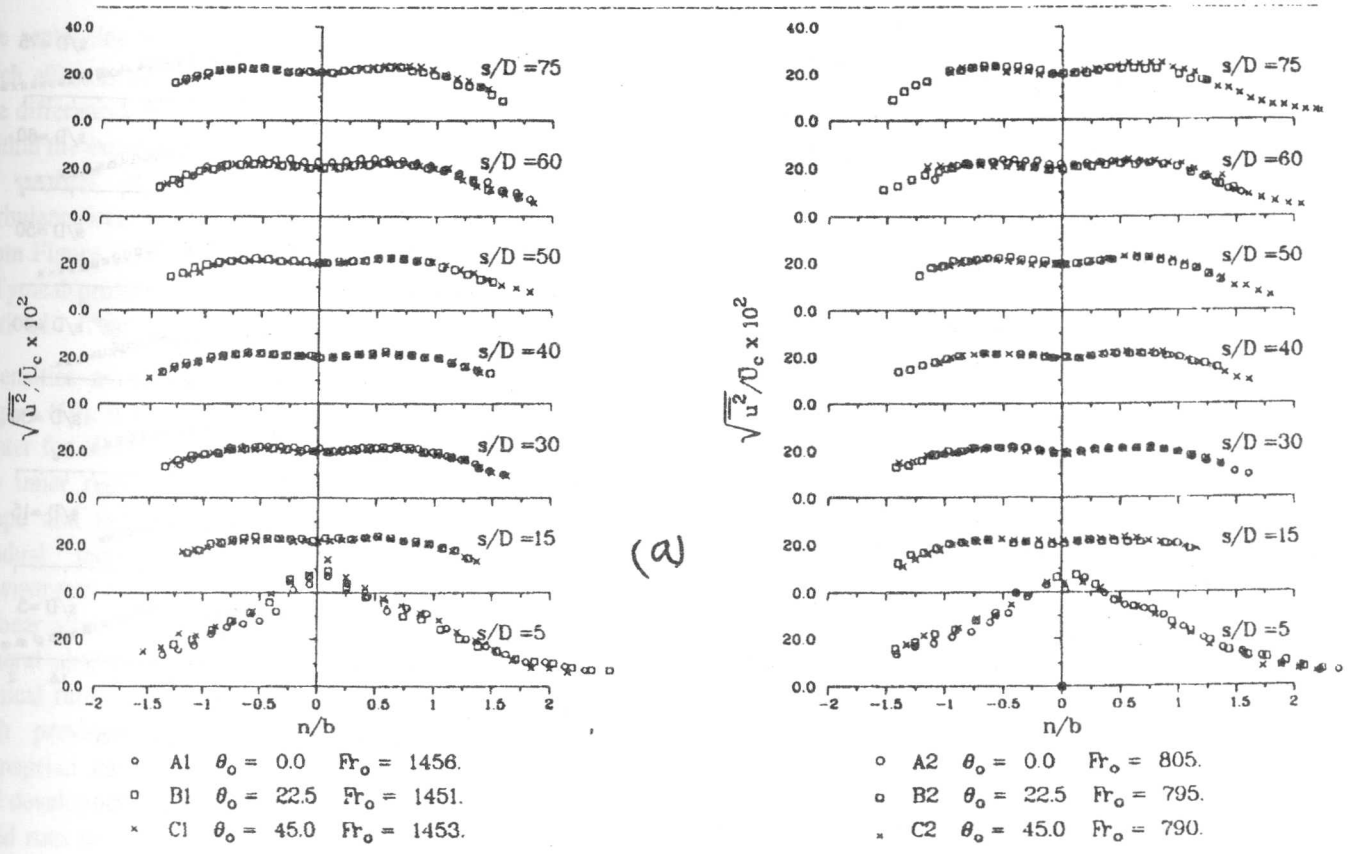

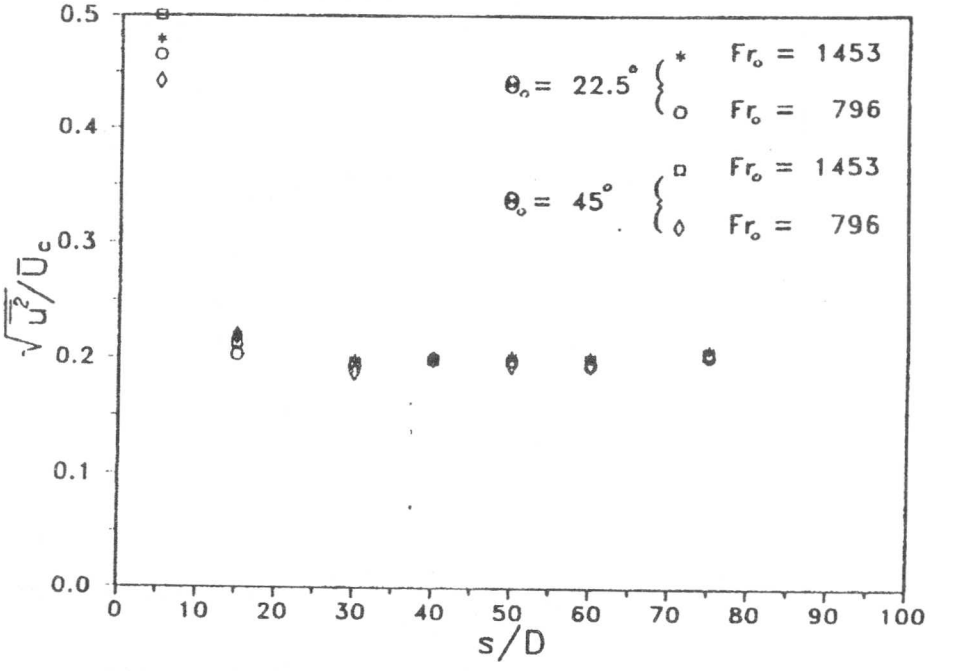

Figure 13. (a) Profiles of longitudinal turbulence intensity.
(b) Center-line variation of longitudinal turbulence intensity.

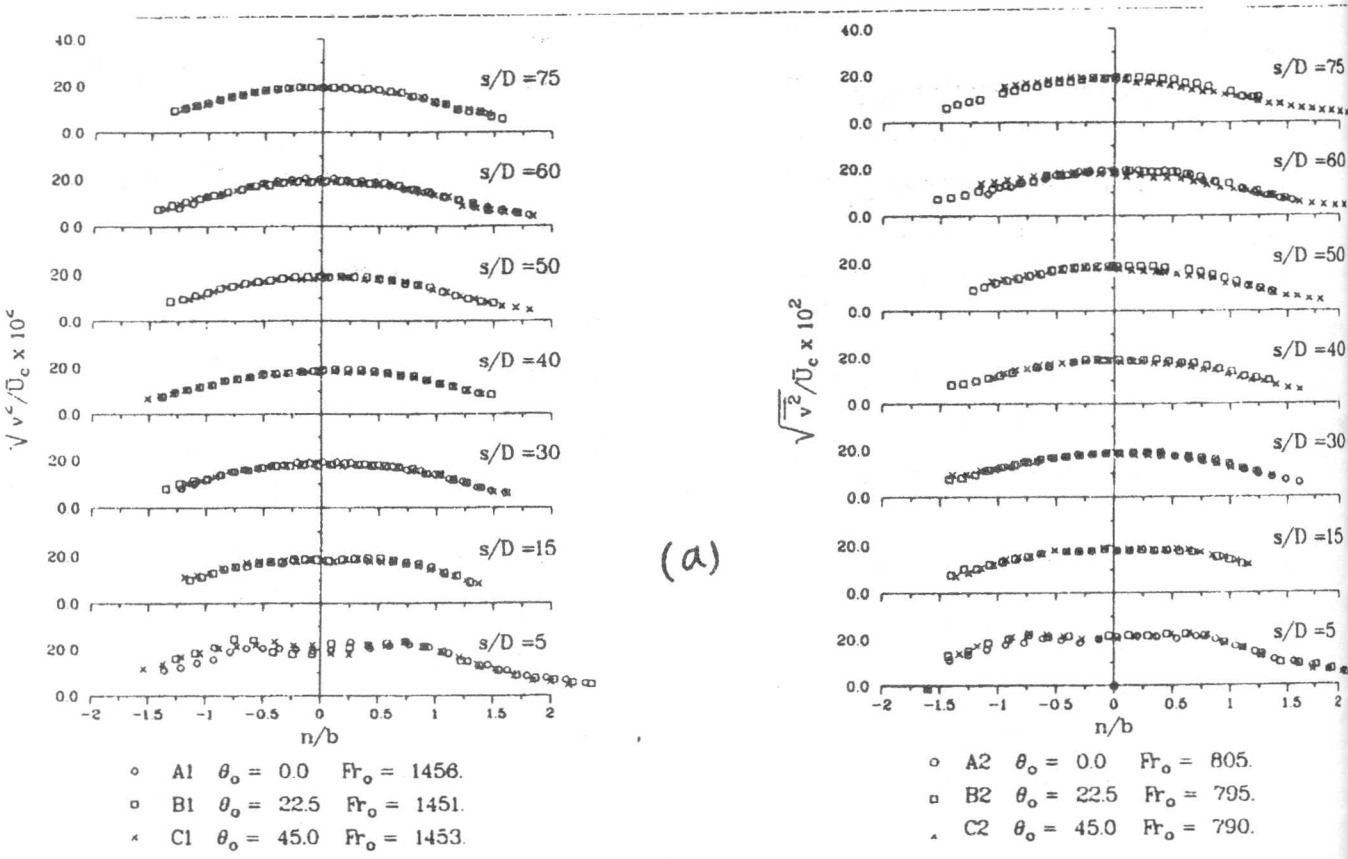

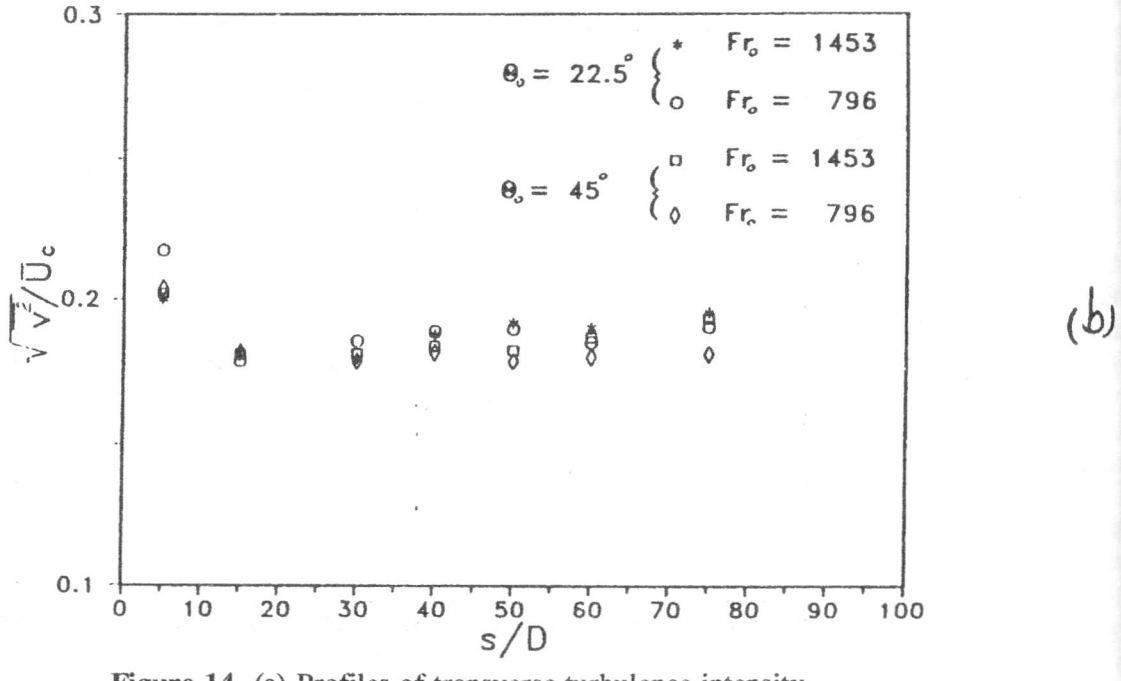

Figure 14. (a) Profiles of transverse turbulence intensity.
(b) Center-line variation of transverse turbulence intensity.

Although the discharge angle shows a slight effect on the center-line variation of $\sqrt{\overline{v^2}}/\bar{U}_c$, a clear trend of such effect is difficult to conclude, particularly, since the differences in the turbulence levels of all runs are within the experimental uncertainty (6.5%). Symmetry of profiles of both longitudinal and transverse turbulence intensities around jet center-line can be seen from Figure (15).

Typical profiles of the turbulence kinetic energy, k, derived from the measurements of turbulence intensities as $k = .5\ (\overline{u^2}+2\overline{v^2})$ are presented in Figure (16). It is seen that the profiles do not peak off-center for all rns, showing a fairly constant T.K.E. in the inner region. The profiles, exhibiting the same shape and symmetry about the center-line, show a gradual increase on the center-line with the downstream distance.

Shear stress profiles are given in Figure (17). The general shape and magnitude of the profiles of the vertical runs (A1 and A2) appear to agree reasonably with previous works (e.g. Chandrasekhara and Ramaprian 1983, Reardon 1985, Sarh et al 1986), and still developing in the downstream distance, s. For the tilted runs the effect of buoyancy and discharge angle (curvature) is more profound than it was found on the other turbulence quantities. This can obviously the seen in the last 3 or 4 stations in runs C1 and C2. The shear stress there was enhanced on the concave (unstable) side of the jet and suppressed on the convex (stable) side. This indicates that instability strengthens the correlation between the fluctuating velocities u and v while stability tends to weaken it. It is observed that the point of zero shear stress (clearly seen in run C2) moved away from the center-line of the jet. This behaviour was also observed by Lemieux (1983). It is also worth pointing out that So and Mellor (1973), in their experiments on an isothermal boundary layer over a convex surface, observed the same behaviour about the point of zero shear stress. They found that the shear stress vanished about midway between the wall and the edge of the boundary layer where there existed a velocity gradient. At station s/D =75 of the run C2, the shear stress is seen to be severally suppressed on the convex (stable) side. The results of measurements of the shear stress correlation coefficient R_{uv}, $R_{uv} = \overline{uv}/(\sqrt{\overline{u^2}}\ \sqrt{\overline{v^2}})$, for a representative downstream station s/d = 60 are shown in Figure (18) and Figure (19) for Fr_o = 796 and 1453 respectively. On the unstable side, R_{uv} is seen to increase with increasing jet discharge angle, thus reflecting the enhancement and strength of turbulence activity there. On the stable side R_{uv} decreases, indicating suppression of turbulence activity. It is to be noted that the maximum values of the shear stress correlation coefficients and their locations for the vertical cases are in good agreement with those for isothermal plane jets (e.g. Gutmark & Wygnanski 1976 and Heskestad 1965).

Profiles of normalized rms temperature fluctuations and its variation along the center-line are presented in Figure (20). It can be observed (particularly from the ceneter-line variation) that the temperature field did not reach self-similarity; the temperature fluctuations are still developing in the downstream direction. A slight dependence can also be observed on the buoyancy forces; the higher the buoyancy forces the higher the temperature fluctuations. No observable dependence of the discharge angle on the temperature fluctuations can be seen.

Typical profiles of normalized heat flux are presented in Figure (21), along with its variation along the jet center-line. The profiles take the characteristic saddle shape as those of the longitudinal turbulence intensity. The profiles are somewhat similar in all the cases, thus showing no clear effect of buoyancy or discharge angle. It is clearly seen that the longitudinal heat flux did not reach self-similarity and is still increasing in the downstream direction. It is difficult from the figure to conclude any significant effect of buoyancy or the discharge angle on the center-line heat flux.

Typical normalized profiles of the transverse heat flux and its variation along the jet center-line are shown in Figure (22). The profiles in almost all the cases are similar in shape but for the run C2, a noticeable effect of buoyancy and discharge angle can be seen. The point of zero heat flux also moved away from the center-line. On the stable side of the jet (convex side), the transverse heat flux was decreased, while, on the unstable side (concave side) it was increased. This again indicates to an increased mixing on the stable side.

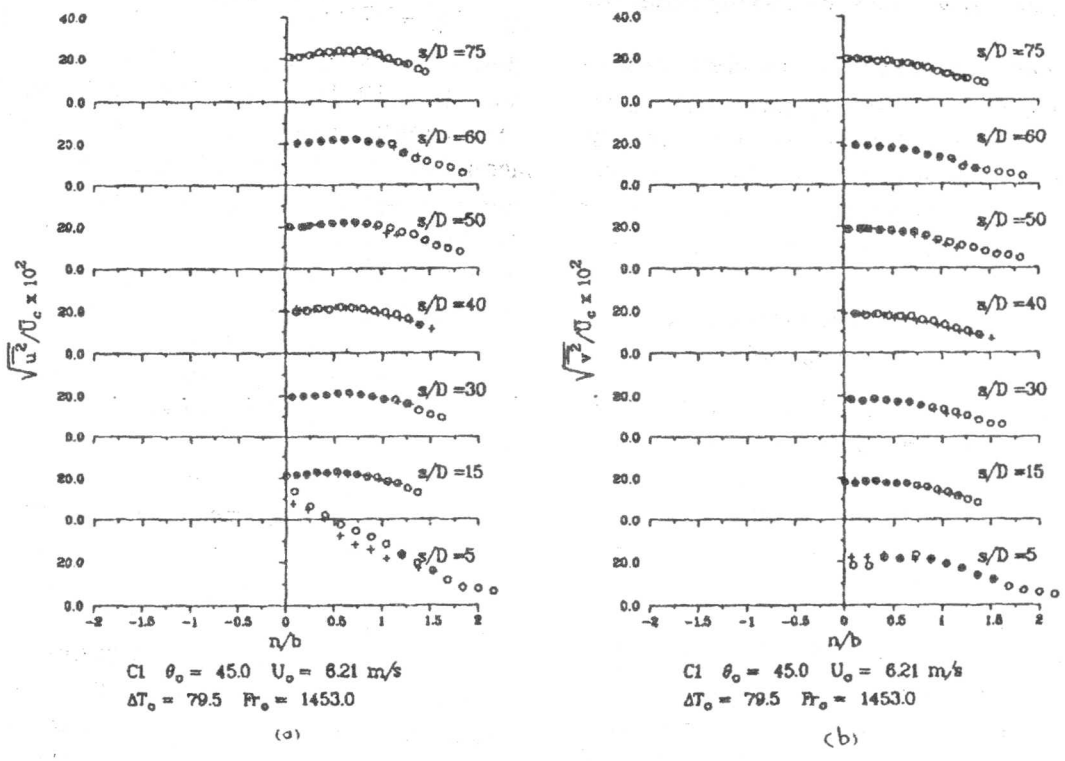

Figure 15. Symmetry of turbulence intensities around jet center-line.
(a) Longitudinal (b) Transverse

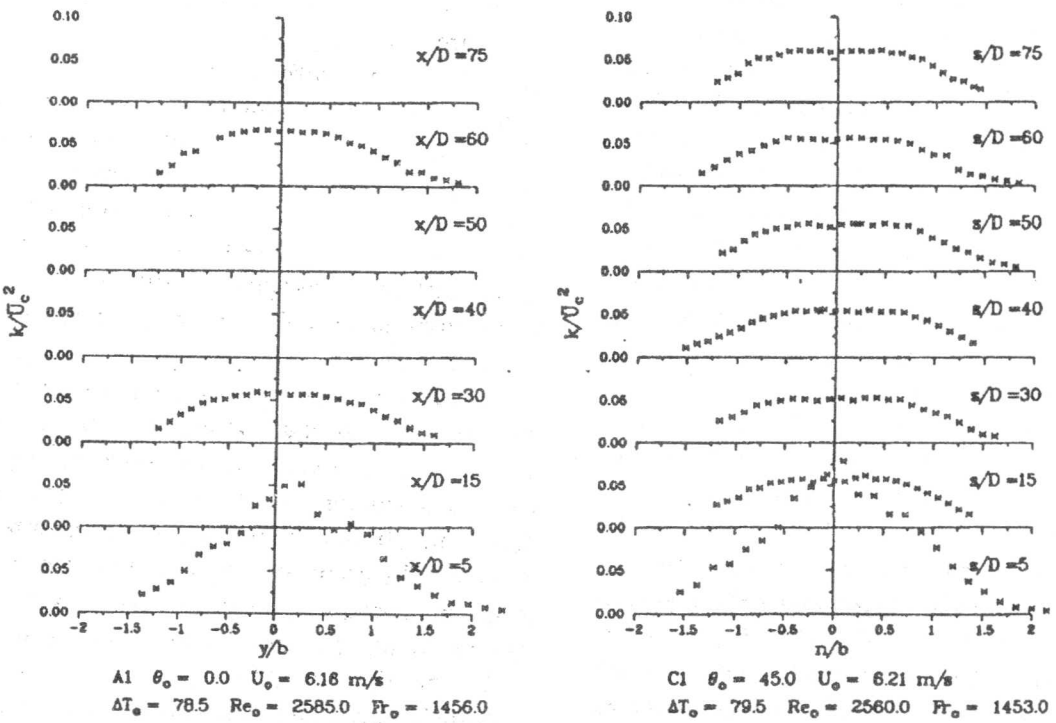

Figure 16. Profiles of turbulence kinetic energy

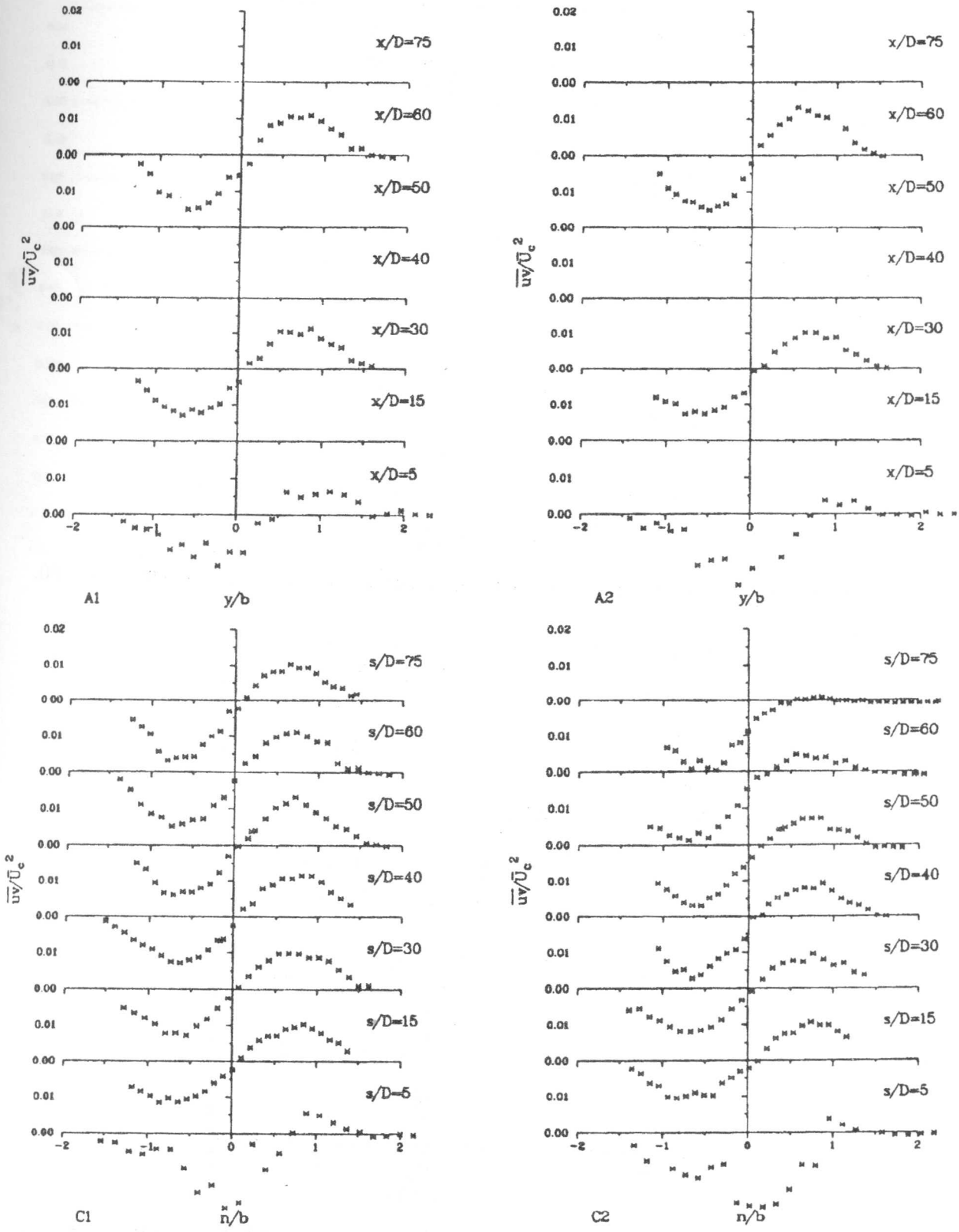

Figure 17. Profiles of turbulence shear stress

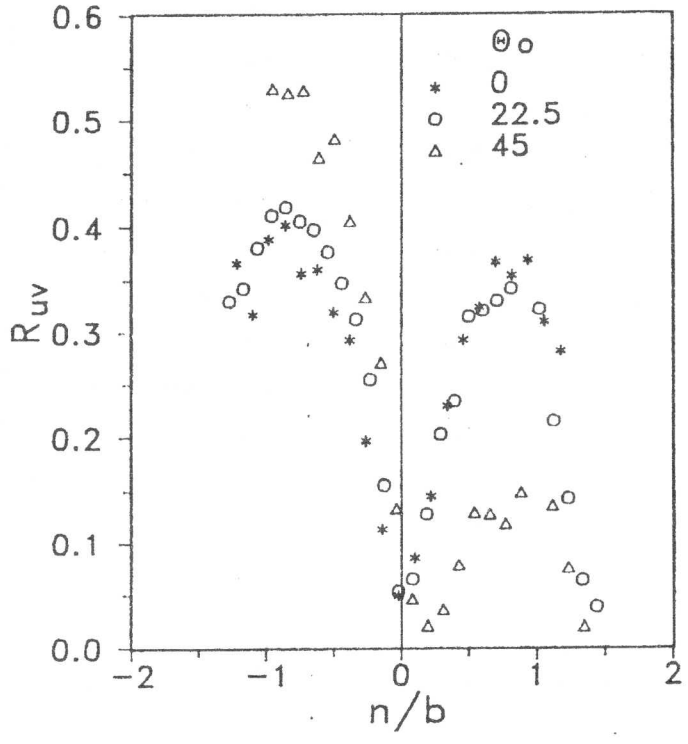

Figure 18. Variation of shear stress correlation coefficient across the jet. Fr_o = 496, s/D = 60.

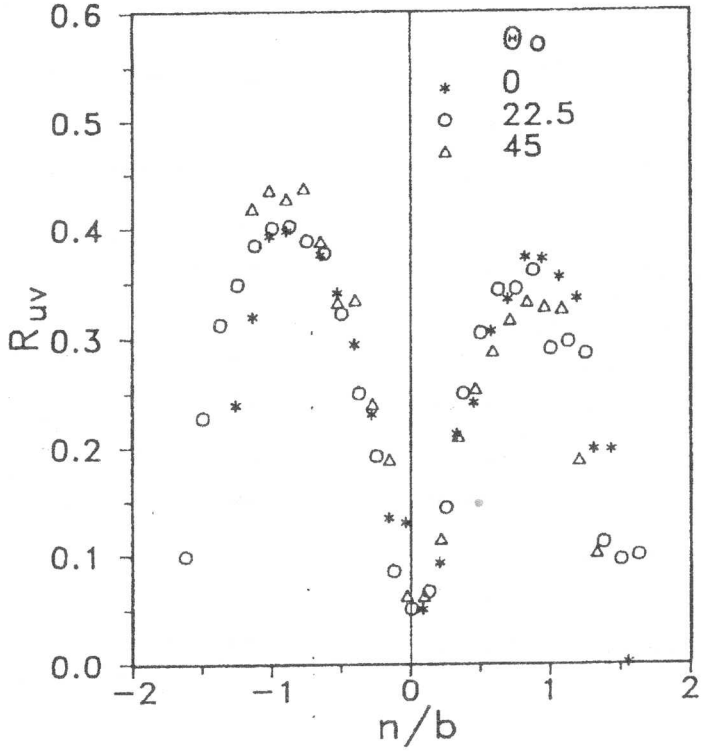

Figure 19. Variation of shear stress correlation coefficient across the jet. Fr_o = 1453, s/D = 60.

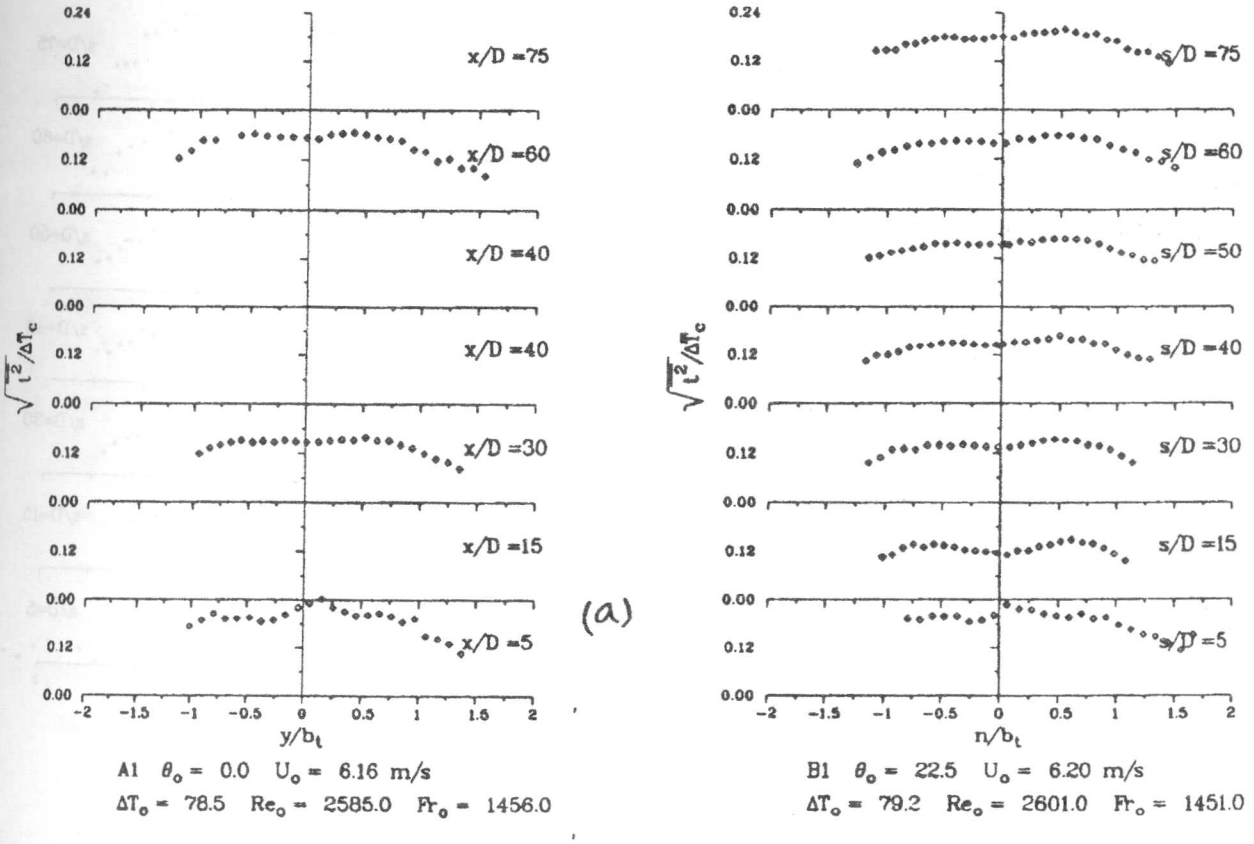

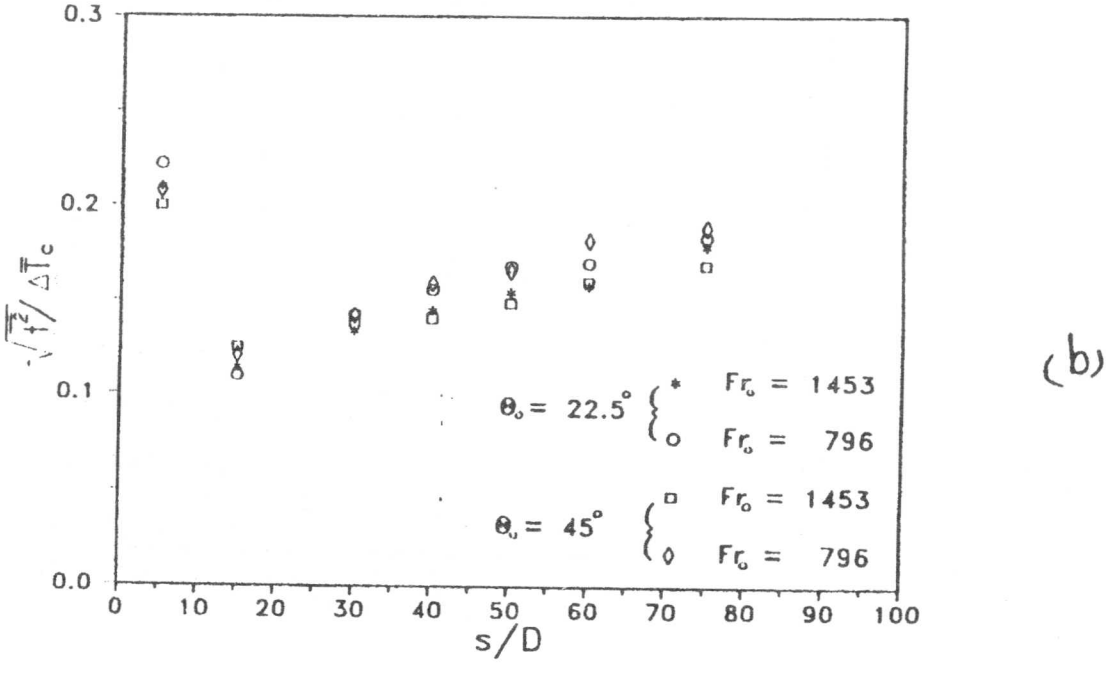

Figure 20. (a) Profiles of rms temperature fluctuations.
(b) center-line variation of rms temperature fluctuations.

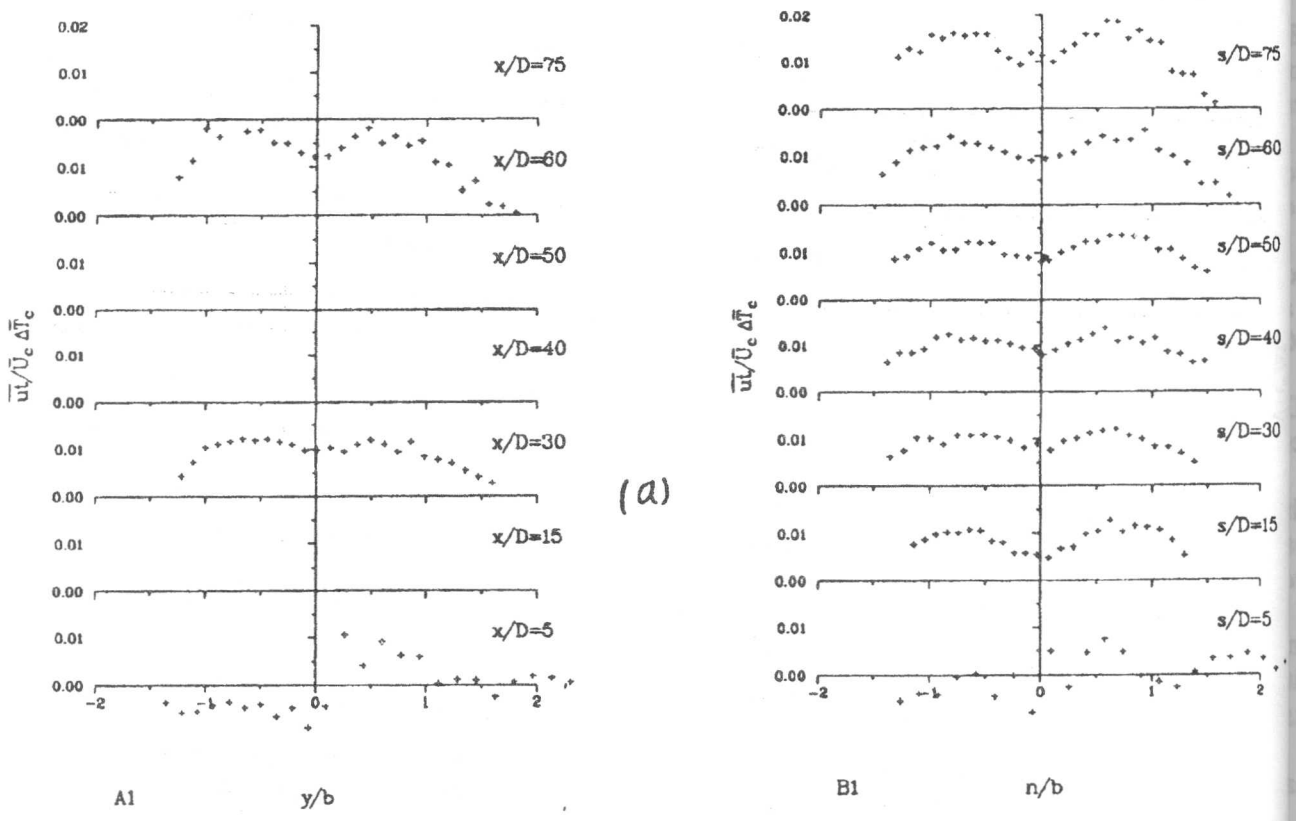

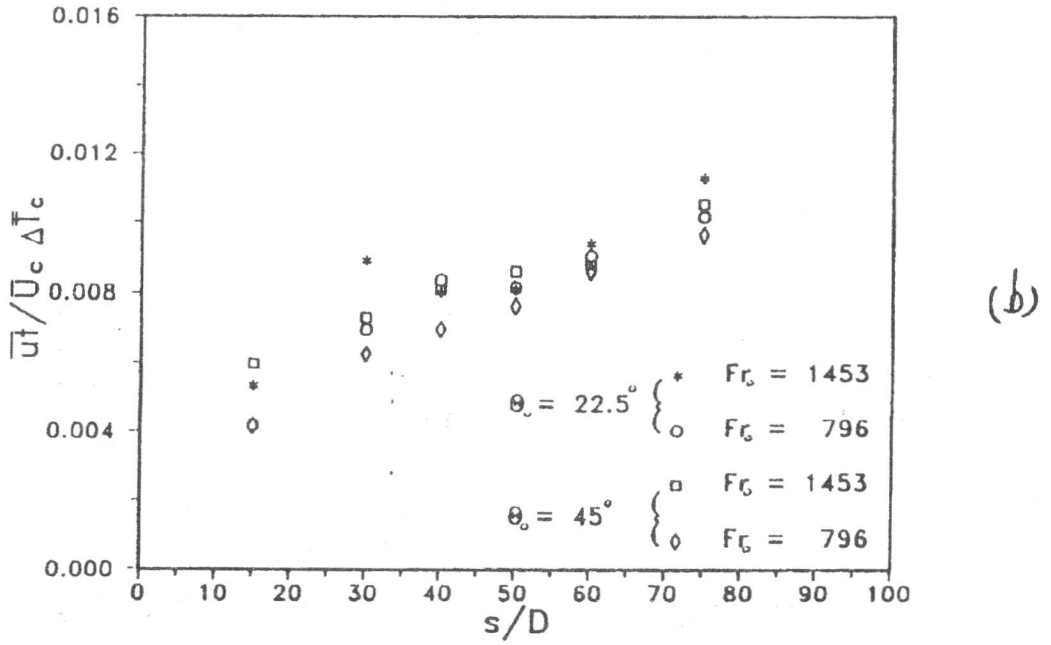

Figure 21. (a) Profiles of longitudinal turbulence heat flux.
(b) center-line variation of longitudinal turbulence heat flux.

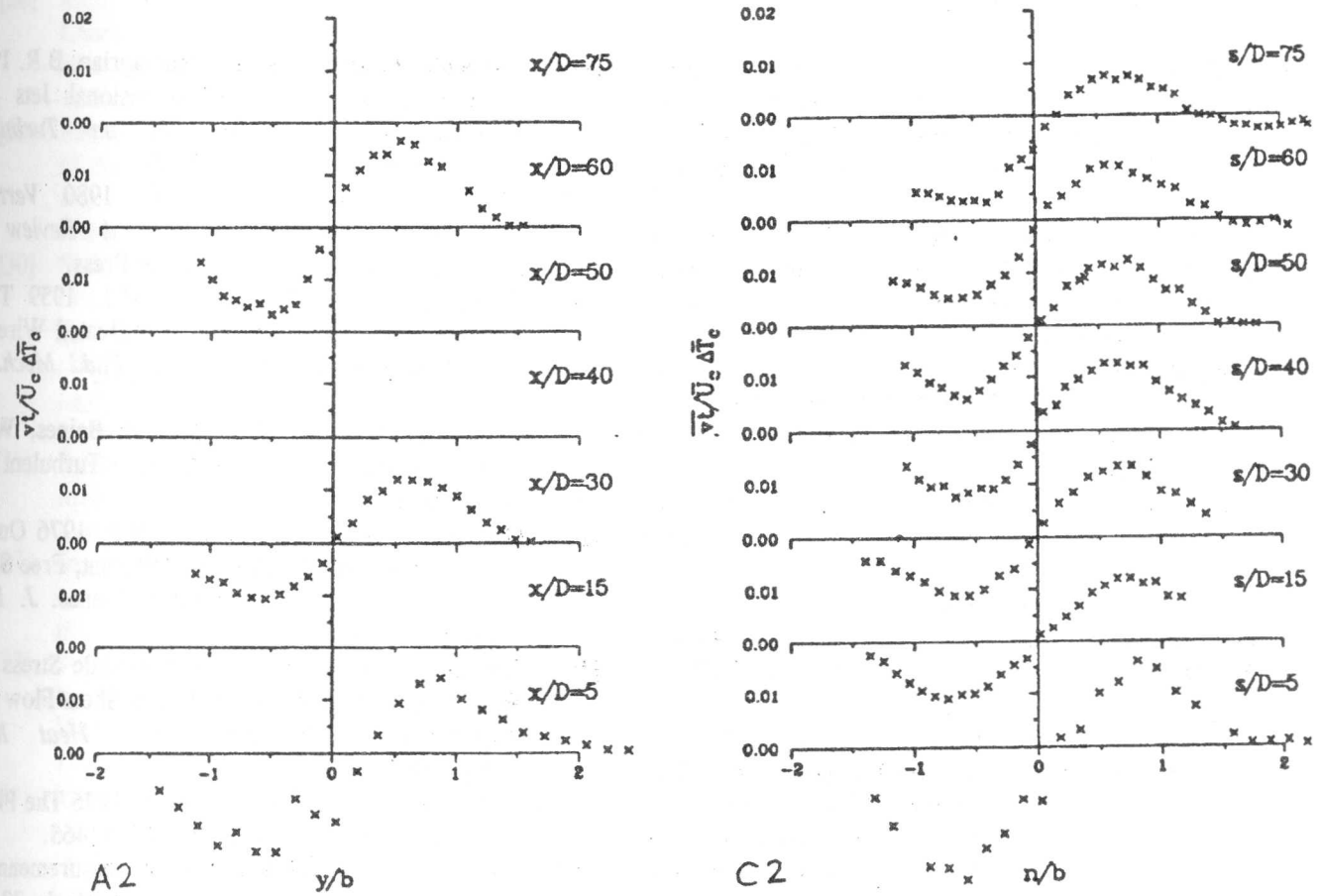

Figure 22. Profiles of transverse turbulence heat flux.

5. CONCLUDING REMARKS

For the range of variable studied in the present investigation, the following may be concluded insofar as applicable to the initial and intermediate regions of the jet flow.

- The mean field of the curved buoyant jet is largely unaffected by either buoyancy forces or discharge angle; the transverse profiles of mean velocity and temperature are basically symmetric around the jet center-line and self-similar for s/D $\geq$ 15.
- Profiles of transverse mean velocity do not exhibit a self-similar from. In the far s/D stations the magnitude of $\bar{V}$ gradually increases on the unstable (concave) side of the jet, and decreases, till ultimately changes sign, on the stable (convex) side. This is due to the suppression of interaction between the jet flow and surrounding air on the stable side and enhancement of such interaction on the unstable side, which indicates to the complexity and difference of the entrainment mechanisms on either side of the jet flow.
- The turbulent quantities most affected by discharge angle/buoyancy are the turbulent shear stress and the transverse heat flux. They gradually decrease on the stable side of the jet and increase on the unstable side. This effect becomes more significant with increasing discharge angle or buoyancy force. The points of zero shear stress and zero transverse heat flux (for some far-field profiles) moved away from the jet center-line.

REFERENCES

[1] Abdel-Rahman, A.A. 1987 An Experimental Investigation of a Buoyant Turbulent Plane Jet with Streamline Curvature. Ph.D. Thesis, University of Waterloo, Waterloo, Ontario, Canada.

[2] Abdel-Rahman, A.A., Tropea, C., Slawson, P. & Strong, A. 1987 On Temperature Compensation in Hot-Wire Anemometry. *J. Phys. E: Sci. Instrum.* 20 (3), 315.

[3] Abdel-Rahman, A.A., Hitchman, G.J., Slawson, P.R. and Strong, A.B. 1989: An X-array Hot-Wire Technique for Heated Turbulent Flows of Low Velocity. J. Phys. E: Sci. Instrum. 22, 638.

[4] Abraham, G. 1965 Horizontal Jets in Stagnant Fluid of Other Density. *J. Hyd. Division, ASCE.* 91 (4), 139.

[5] Anwar, H.O. 1969 Experiment on an Effluent Discharging from a Slot into Stationary or Slow-Moving Fluid of Greater Density. *J. Hyd. Res.* 7 (4), 411.

[6] Bashir, J. & Uberoi, M. 1975 Experiments on Turbulent Structure and Heat Transfer in a Two-Dimensional Jet. *Phys. Fluids.* 18 (4), 405.

[7] Bradshaw, P. 1971 *An Introduction to Turbulence and Its Measurements. Pergamon* Press.

[8] Bruun, H.H. 1971 Interpretation of a Hot-Wire Signal Using a Universal Calibration Law. *J. Phys. E: Sci-Instrum.* 4, 225.

[9] Bruun, H.H. 1972 Hot-wire Data Correction in Low and High Turbulence Intensity Flows. *J. Phys. E: Sci. Instrum.* 5, 812.

[10] Bruun, H.H. & Tropea, C. 1985 The Calibration of Inclined How-Wire Probes. *J. Phys. E: Sci. Instrum.* 18, 405.

[11] Buresti, G. & Cocco, N.R.Di. 1987 Hot-wire Measurement Procedures and Their Appraisal Through a Simulation Technique. *J. Phys. E: Sci. Instrum.* 20, 405.

[12] Champagne, F.H., Sleicher, C.A. & Wehrmann, O.H. 1967 Turbulence Measurements with Inclined Hot-Wires (Part 1. Heat Transfer Experiments with Inclined Hot-Wire). *J. Fluid Mech.* 28, 153.

[13] Chan, T.L. & Kennedy, J.F. 1972 Turbulent Non-Buoyant or Buoyant Jets Discharged into Flowing or Quiescent Fluids. *IIHP Report no. 140.* The University of Iowa.

[14] Chandrasekhara, M.S. & Ramaprian, B.R. 1 Measurements in Two-dimensional Jets Plumes. *4th Symposium on Turbu Shear Flows.* Karlsruhe, FRG.

[15] Chen, C.J. & Rodi, W. 1980 *Ver Turbulent Buoyant Jets - A Review Experimental Data. Pergamon* Press.

[16] Collis, D.C. & Williams, M.J. 1959 T dimensional Convection from Heated Wire Low Reynolds Numbers. *J. Fluid Mech.* 357.

[17] Davies, A.E., Keffer, J.F. & Baines, W 1975 Spread of a Heated Plane Turbulent *Phy. Fluids.* 18 (7), 770.

[18] Gibson, M.M. & Launder, B.E. 1976 On Caculation of Horizontal Turbulent, Free Sh Flows under Gravitational Influence. *J. H Transfer.* 19, 81.

[19] Gibson, M.M. 1978 An Algebraic Stress Heat-Flux Model for Turbulent Shear Flow Streamline Curvature *I.J. Heat M Transfer* 21, 1609.

[20] Gutmark, E. & Wygnanski, I. 1976 The Pla Turbulent Jet. *J. Fluid Mech.* 73, 465.

[21] Heskestad, G. 1965 Hot-Wire Measurement a Plane Turbulent Jet. *J. Appl. Mech.* 32 721.

[22] Hinze, J.O. 1975 *Turbulence.* New Y McGraw Hill Book Co.

[23] Hussain, A.K.M.F. & Clark, AR. 1 Upstream Influence on the Near Field of a Pl Turbulent Jet. *Phy. Fluids.* 20 (9), 1416.

[24] Kotsovinos, N.E. & List, E.J. 1977 Pl Turbulent Buoyant Jets (Part 1, Inte Properties & Part 2, Turbulence Structure) *Fluid Mech.* 81, 25.

[25] Mobarak, A., Sedrak, M.F. & Telb M.M.M. 1986 On the Directional Sensitivity Hot-Wire Probes. *Dantec Infor. no* 2.

[26] Otugen, M.V. & Namer, I. 1986 The Effec Reynolds Number on the Structure of Pl Turbulent Jets. *AIAA 24th Aerosp Sciences Meeting.* Reno, Nevada.

[27] Oosthuizen, P.H. & Lemieux, G.P. 1984 Experimental Study of an Inclined Buoy Plane Turbulent Air Jet. *ASME Heat Tran* Conference. AIAA 24th Aerospace Scien Meeting, Reno, Nevada.

[28] Rajagopalan, S. & Antonia, R.A. 1980 Characteristics of a Mixing Layer of a Two-Dimensional Turbulent Jet. *AIAAJ*. 18 (9), 1052.

[29] Reardon, J. 1985 AN Experimental Investigation of the Turbulence Structure of a Heated Plane Jet. Ph.D. Thesis, University of Waterloo, Waterloo, Ontario, Canada.

[30] Sarh, B., Gokalp, I.& Fulachier, L. 1986 Investigations on the Dynamic Field of a Strongly Heated Turbulent Rectangular Jet. *3rd Int. Symposium on Applications of Laser Anemometry to Fluid Mechanics.* Lisbon, Portugal.

[31] Schwartzbach, C. 1972 An Experimental Investigation of Curved Two-Dimensional Turbulent Jets *AGARD Conf. Proc.*, 93.

[32] So, R.M.C. & Mellor, G.L. 1973 Experiment on Convex Curvature Effects in Turbulent Boundary Layers. *J. Fluid Mech.* 60 (1), 43.

[33] Swaminathan, M.K., Rankin, G.W. & Sridhar, K. 1986 A Note on the Response Equations of Hot-Wire Anemometry. J. *Fluid Engng, Trans. A.S.M.E.* 108, 115.

[34] Verriopoulos, C.A. 1983 Effects of Convex Curvature on Heat transfer in Turbulent Flow. Ph.D. Thesis, Imperial College, London, England.